Ocean Modelling 81 (2014) 36–48

Contents lists available at ScienceDirect

Ocean Modelling

journal homepage: www.elsevier.com/locate/ocemod

A realistic freshwater forcing protocol for ocean-coupled climate models

J. van den Berk [a,*], S.S. Drijfhout [b,a]

[a] Royal Netherlands Meteorological Institute, De Bilt, The Netherlands
[b] School of Ocean and Earth Science, University of Southampton, Southampton, United Kingdom

ARTICLE INFO

Article history:
Received 6 December 2013
Received in revised form 10 July 2014
Accepted 16 July 2014
Available online 25 July 2014

Keywords:
Surface freshwater flux
Global ocean model
North Atlantic
Southern ocean

ABSTRACT

A high-end scenario of polar ice loss from the Greenland and Antarctic ice sheet is presented with separate projections for different mass-loss sites up to the year 2100. For each large ice sheet three potential sources of freshwater release to the ocean are considered: run-off from surface melt, basal melt through heat exchange with the ocean, and iceberg calving and subsequent mass loss through melt of drifting icebergs. The location and relative magnitude of freshwater forcing due to drifting icebergs is calculated from a separate iceberg drift simulation. We assume fixed annual spatial patterns with magnitudes varying in time. These magnitudes are based on a severe warming scenario based on expert elicitation. The resultant freshwater forcing is applied to a global climate model and the effects on sea-level rise are discussed. The simulations show strong sea level rise on the Antarctic continental shelves. The effect on the Atlantic overturning circulation is very small, however.

© 2014 The Authors. Published by Elsevier Ltd. This is an open access article under the CC BY-NC-ND license (http://creativecommons.org/licenses/by-nc-nd/3.0/).

1. Introduction

It is expected that the ice stored on Greenland and Antarctica will diminish during the coming century. The estimates of the amount so far have varied widely (Katsman et al., 2011; Pfeffer et al., 2008; Rignot et al., 2011; Thomas et al., 2009). Nonetheless it seems pertinent to incorporate this mass loss in Coupled Climate Models (CCMs) when making projections of future climate change. A rising global mean temperature is expected to enhance mass loss of both the Greenland and the Antarctic ice sheet Gregory and Huybrechts, 2006. Most of the current CCMs lack an interactive ice sheet model to handle these processes dynamically. As we should take into account this mass loss, we have to model the response of the ice sheets in CCMs in another way. Our intent is to provide a prescription of how this can be done for any ocean model.

An ice sheet's surface mass balance (SMB) is the amount of water gained minus the amount lost. Many processes affect the SMB of an ice sheet; those mentioned in Shepherd et al. (2012) are solid and liquid precipitation, surface sublimation, drifting snow transport, erosion and sublimation, melt-water formation, re-freezing, retention, and run-off. An increased melt might lubricate a glacier and increase its rate of retreat, leading to more iceberg calving (see Greve and Blatter, 2009 for an introduction to the dynamics of glaciers).

Most CCMs do not couple with an interactive ice sheet model and can not be expected to model these mass loss processes due to a warming climate. By prescribing the mass loss, this defect can be compensated for. A prescription based on a plausible high-end sea-level rise scenario is presented with the purpose to be easily implemented in a CCM.

Parametrisations of ice sheet melting do exists (Beckmann and Goosse, 2003; Wang and Beckmann, 2007), but are limited in their scope and applicability to any particular climate model. A similar problem exists with the parametrisation of iceberg calving (Alley et al., 2008; Amundson and Truffer, 2010), where it is often cumbersome to include these parametrisations in an ensemble of different models.

Our manuscript is organised as follows. We begin with identifying the processes at work and their locations. A motivation for the freshwater projections is given in Sections 2 and 3. Details of how the projections should be implemented is explained in Appendix A. The effects on sea-surface height are discussed in Section 4. We end with a summary.

1.1. Model description

We will show some results using the CCM EC-Earth (Hazeleger et al., 2010, 2012) which does not include an interactive ice-sheet module. EC-Earth consists of three computational components. The atmosphere is modelled with the Integrated Forecast System (IFS),

* Corresponding author.
E-mail addresses: jelle.van.den.berk@knmi.nl (J. van den Berk), s.s.drijfhout@soton.ac.uk, sybren.drijfhout@knmi.nl (S.S. Drijfhout).

http://dx.doi.org/10.1016/j.ocemod.2014.07.003
1463-5003/© 2014 The Authors. Published by Elsevier Ltd.
This is an open access article under the CC BY-NC-ND license (http://creativecommons.org/licenses/by-nc-nd/3.0/).

cycle 31r1 which has a resolution of 62 layers in the vertical and triangular truncation at wavenumber 159 ECMWF, 2006 (effectively resolving ≈ 130 km gridded). The ocean is modelled by the Nucleus for European Modelling of the Ocean (NEMO) developed by the Institute Pierre Simon Laplace at a resolution of approximately 1° in the horizontal (≈ 110 km) and 42 levels in the vertical (Madec, 2008). The two are synchronised along the interface every three model-hours by the OASIS3 coupler developed at the Centre Europe en de Recherche et Formation Avances et Calcul Scientifique (Valcke et al., 2004). The ocean model is further extended by a sea–ice module of Louvain-la-Neuve (LIM) (Morales Maqueda and Fichefet, 1997; Morales Maqueda et al., 2009).

The iceberg output used as forcing is derived from a modified version of Bigg et al. (1996, 1997) iceberg model, developed by Martin and Adcroft (2010) and coupled to ORCA025, an eddy-permitting global implementation of the NEMO ocean model (Madec, 2008), to simulate the trajectories and melting of calved icebergs from Antarctica and Greenland in the presence of mesoscale variability and fine-scale dynamical structure.

Icebergs are treated as Lagrangian particles, with the distribution of icebergs by size derived from observations (see Bigg et al., 1997 and Table 1). The momentum balance for icebergs comprises the Coriolis force, air and water form drags, the horizontal pressure gradient force, a wave radiation force, and interaction with sea ice. The mass balance for an individual iceberg is governed by bottom melting, buoyant convection at the side-walls and wave erosion (see Bigg et al., 1997).

This configuration has been run for 14 years, and the associated freshwater fluxes used here are averages over years 10–14. Southern Hemisphere calving and melting rates are in near balance after 10 years, but further decades of simulation would be needed for global balance, due to slower equilibration of calving and melting in the Northern Hemisphere. An average pattern of icebergs is our primary interest, which is why we settled for a relatively short integration time.

2. Mass loss processes and their locations

For our purposes a detailed treatment of various mass loss processes is not necessary, because only the amount of freshwater release applied to the ocean is of interest. Nevertheless, the many different processes that affect the SMB indicate that uncertainties are to be expected and distinction between mass loss processes and geographical locations needs to be made (Shepherd et al., 2012).

The most obvious response to increased atmospheric temperatures is the melting of ice. This mass loss can be associated with adding freshwater directly offshore of the coast of the region where the melt takes place. We designate this freshwater source as *run-off*, or *R* for short. Run-off is contrasted with another form of mass loss that produces icebergs. The calving of icebergs from glaciers we call *ice discharge*, or *D*. The important difference is that icebergs are free floating chunks of ice and can drift to other locations and melt.

This last observation prompts us to introduce the distinction between *near* (*N*) and *far* (*F*) freshwater forcing. A near forcing is always adjacent to the coast of origin and a far forcing is not restricted like this.

The output of the iceberg drift and melt simulation gives us the location and relative magnitude of the far source of freshwater forcing. We assume spatial patterns on an annual cycle for these contributions, with magnitudes varying in time. The scaling factors are provided by the mass loss projections in the two polar regions.

Glaciers not only calve blocks of ice, but (relatively) warm ocean water will also melt tidewater glaciers when the two are in contact. This is called basal melt (*B*) and takes place within the shelf cavity. The ice discharge not melted away we call the *ice flux* (*I*). Basal melting affects all glaciers and ice shelves but the extent is determined by the local temperature of the water. Floating ice shelves loose mass by the relatively warm ocean water compared to the freezing point (Rignot and Jacobs, 2002). This melt contribution to freshwater release into the ocean is relatively small compared to other forms of melt. Mass loss as a result of floating ice shelves does not contribute to sea level rise (Jenkins and Holland). However, in general (in equilibrium) this mass loss is balanced by ice discharge from the grounded part of the glacier. If basal melt actually forms a significant part of the ice discharge from the glaciers the full *D* can not be treated as only due to iceberg calving. A fraction of *D* is released as freshwater run-off at the glaciers' calving face and the remainder is left available to drift away in the form of icebergs. A certain fraction of *D* is added to *N* with the remainder allocated to *F*. (For a schematic overview of these labels see Fig. 1.)

In this section we will identify the regions we wish to treat separately on the basis of the different characteristics of mass loss (processes) that differentiate them. We start by noting that Greenland and Antarctica are the locations of the polar ice caps and proceed from there. We list important characteristic values (at present day) where appropriate. In particular these will be basal melt fractions (the fraction of the iceberg melted away before it is adrift, or μ), and mass loss. Projections of future development of mass loss are constructed in Section 3.

Both Greenland and Antarctica are covered by ice sheets, but also differ substantially. Firstly, Antarctica stores a considerably larger amount of ice (Hanna et al., 2008; Van Den Broeke et al., 2011). Secondly, Greenland melt is expected to increase with a decreasing surface mass balance (Hanna et al., 2008), whereas Antarctica could also gain mass in the future (Church et al., 2013). A third reason to distinguish between the two regions is the type of glacier present. On this basis we subdivide further and segment

Table 1
Greenland tidewater glaciers used to define regions i and ii. (See Rignot and Kanagaratnam, 2006 for an overview for Greenland glacial mass loss.)

Glacier	D_{init} (Gt/yr)	
Region i		
(a) Jakobshavn Isbræ	27	
(b) Petermann	12.2	
(c) Ryder	4.3	
(d) Nioghalvfjerdsbræ	14.3	
(e) Zachariæ Isstrøm	11.7	
		69.5
Region ii		
(f) Helheim	26.2	
(g) Ikertivaq	10.3	
(h) Storstrømmen	6.8	
(i) Daugaard-Jensen	10.5	
(j) Kangerdlugssuaq	27.9	
		81.7

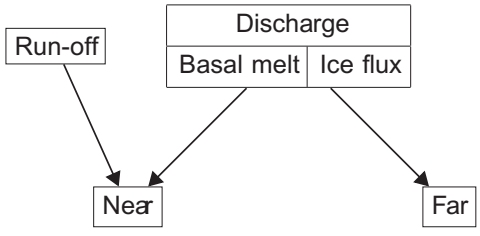

Fig. 1. Schematic overview of mass-loss processes and their re-labelling.

Greenland and Antarctica in smaller sections, each with their own storyline.

2.1. Greenland

Greenland is expected to experience increased surface melt as well as increased iceberg calving from its tidewater glaciers Katsman et al., 2008. The three main tidewater glaciers we need to consider are Jakobshavn Isbræ in the west and Kangerdlugssuaq and Helheim in the east (Rignot and Kanagaratnam, 2006) (see Fig. A.10 for their locations). Smaller tidewater glaciers are located in the north. Glaciers with relatively small discharge values are ignored (Katsman et al., 2011). The glaciers in Table 1 not explicitly mentioned are simply taken to be part of the region listed. A distinction must be made between the glaciers with termini that are expected to retreat to above sea-level and those that are not expected to do so during the coming century. The foremost example of a glacier whose terminus will not retreat is Jakobshavn Isbræ, but the northern glaciers' topography also prevent this (Katsman et al., 2008). We then arrive at separate scenario projections, which roughly divide Greenland into three regions. The first (n_{i}) will consist of the northern tidewater glaciers and Jakobshavn Isbræ, which have non-retreating termini. The second region (n_{ii}) covers the eastern tidewater glacier. These do have retreating termini. The third (n_{iii}) region is the remainder, where surface melt is the primary mass loss process. The glaciers that make up regions i and ii are listed in Table 1.

2.2. Recent Greenland melt

There are three major glaciers in Greenland that will be considered here: Helheim, Kangerdlugssuaq and Jakobshavn. Of these, Helheim and Kangerdlugssuaq do not have developed ice tongues[1] (Thomas et al., 2009). Jakobshavn does have an ice tongue and for this reason a substantial basal melt fraction is to be expected there. A related reason is that Jakobshavn has a sill before its flux gate that can trap the (warm) water that moves past it, and it is hypothesised that this helps to increase the glacier's flow rate (Holland et al., 2008; Rignot et al., 2010), supported by the findings of Motyka et al. (2011). A basal melt fraction of $\mu = 0.29$ for the Jakobshavn Isbræ was found (Motyka et al., 2011) before its ice tongue broke off in 2003. The ice tongue inhibits calving, but due to a larger surface area, also enhances basal melt. More recent observations indicate that the area of the glacier that is thinning is reaching ever further inward (Thomas et al., 2009). This is found to be the case for the three major Greenland glaciers, but Kangerdlugssuaq and Helheim show great variability (Thomas et al., 2009). Glaciers that are part of the hydrological cycle, but are not expected to increase their mass loss (see Katsman et al., 2011), are ignored.

Other measurements of basal melt flux of three of Greenland's western glaciers are given in Rignot et al. (2010). The glaciers run deep and have shallow sills that limit exchange of water with the adjoining ocean. A range of μ = 0.2–0.8 is found for the summer basal melt. These glaciers might not be representative for the larger western Greenland region, and the large variation in melt fraction indicates critical dependence on local circumstances.

On the basis of these findings, we will assume the same basal melt fractions for two of the three regions of Greenland. We assume that the northern part suffers no basal melt, because of the relatively low thinning rates found there (Thomas et al., 2009). The other two regions are associated with (mostly) tidewater glaciers, and the geographical similarity implies that we also expect similar temperature rise in sea water. The authors of Thomas et al. (2009) find that especially glaciers with bed topography well below sea-level (hundreds of metres) are thinning rapidly.

The values given in Rignot et al. (2010) are for summer only. Assuming two seasons of equal duration we take halve of these values to be appropriate annual means. The average ($\mu = 0.25$) is also comparable to the earlier quoted value of 0.29 for Jakobshavn Isbræ in the mid 1980s. If we assume, on the basis of thinning rates, that a similar basal melt rate applies here we can use 0.25 for the relevant Greenland regions (n_{ii} and n_{iii}).

2.3. Antarctica

Like Greenland, Antarctica has varying geography that leads to a different treatment of each sub-region. In Katsman et al. (2008), three areas that are at risk of enhanced mass loss are identified. The first is the Amundsen Sea Embayment (ASE i, taken to correspond to Pine Island and Twaites), which feeds the west Antarctic Ice Sheet (WAIS). The second area consists of Totten glacier, Cook ice-self glacier and Denman glacier (ii), which are large marine ending glaciers feeding the east Antarctic Ice Sheet (EAIS). The final region (iii) is the north Antarctic Peninsula (N-AP). Other ice shelves that might be at risk are the Filchner Ronne and Brunt ice shelf (Hellmer et al., 2012). As will be shown below, our implementation can easily take into account initial mass loss, if such a storyline is considered appropriate.

2.4. Recent Antarctica melt

Basal melt rates have been determined for various Antarctic glaciers in Rignot and Jacobs (2002). The values we use are the grounding line ice flux and a downstream flux gate, as given in their Table 1. If no basal melt were to occur, then the difference between these two quantities would be zero (assuming no accumulation or other ablation occurs as these authors do). The difference is then equal to the amount of melt that has occurred between the grounding line and the gauge flux gate. We will name this difference $\Delta\phi$ and let $\mu = \Delta\phi/D$. We will summarise the findings in Rignot and Jacobs (2002) per region in the following paragraphs. We only discuss those regions and glaciers that are expected to show a (substantial) increase in discharge by Katsman et al. (2011). Those glaciers that are ignored do not contribute to additional melt, but can still play a (substantial) part in the hydrological cycle.

WAIS. The west Antarctic Ice Sheet (taken to correspond to the glaciers Pine Island, Thwaites, Smith and Crosson, and Kohler and Dotson in Rignot and Jacobs (2002)) shows $\Delta\phi = 59.5$ Gt/yr. The same region showed an ice discharge, $D = 215$ Gt/yr. The melt ratio for this region is $\mu_{s_{\mathrm{i}}} = 59.5/215 \approx 0.30$. More recent measurements (Rignot et al., 2013) indicate that a larger melt ratio perhaps is more appropriate. However, we will keep the lower value here.

EAIS. The value given for the eastern ice sheet region is $152 - 93.3 = 58.7$ Gt/yr of basal melt, or $\mu_{s_{\mathrm{ii}}} = 0.15$ (Rignot and Jacobs, 2002).

N-AP. The northern peninsula region is not explicitly taken into account in Rignot and Jacobs (2002), but the area geographically closest to it (Evans and Ronne ice shelf) is given to have a basal melt rate of 31.7 Gt/yr, and the corresponding region in Rignot et al. (2008) (IH', English Coast) has a 1996 ice discharge of 78 Gt/yr. We then find $\mu_{s_{\mathrm{iii}}} = 0.40$. The basal melt ratios for the Antarctic ice discharge are substantial and regionally dependent on local temperature. This is elaborated in Rignot and Jacobs (2002) where a 1 K increase leads to an increase of 10 m/yr in the basal melt rate.

[1] A floating protrusion of ice from a glacier which has a relatively large surface area exposed to the ocean water.

For Jakobshavn Isbræ we found a considerable basal melt fraction, on par with the value found in the western Antarctic. The putative values for the six scaling regions (three Greenland and three Antarctic regions that have mass loss values controlled independently from each other) considered are listed in Table 2.

2.5. Deposition area of freshwater release

The amount of basal melt is strongly connected to the characteristics of the donor glacier and for this reason it would be unreasonable to simply spread this freshwater along the entire Greenland coast. We restrict the deposition to an area close to the source glacier, and prescribe it as a mass flux at the surface. The details of the horizontal distribution are given in Appendix A.

In Greenland, the major tide-water glaciers are Jakobshavn in the west, and Kangerdlugssuaq and Helheim in the east. The total amount of Greenland ice discharge is based on Rignot and Kanagaratnam (2006) where a list of glaciers is provided. The location of the given glaciers can be used to determine where the basal melt component of the freshwater flux is to be placed. The same procedure can be used for Antarctica. The discharge values we use are taken from Rignot et al. (2008).

Because basal melt manifests itself as a freshwater forcing already at the calving face, the corresponding fraction of D should be applied to the coastal grid-cells. The effect is that the amplitude of the ice discharge diminishes regionally, and is replaced by an *effective* run-off component in the form of the near forcing. The far forcing will be given by iceberg melt and is typically further from the coast.

3. Mass loss scenarios and projections

A scenario consists of a storyline of some events to come (Katsman et al., 2011). A projection is the future evolution of a particular variable (mass loss) based on a certain scenario. In the case of sea-level rise, this implies a quantification of the amount of additional water at a particular point in time (often the year 2100) added to the ocean. Since we not only want to consider an accumulated loss, but also the progression in time, we will suggest time-dependent projections of mass loss for each region identified above. Firstly we treat the implications of the storyline given in Katsman et al. (2011) for Greenland followed by the one for Antarctica. The conversion values in Table 3 can be used to convert between common units. For each scaling region a separate projection will be given.

The basal melt seems to relate directly to calving rates and not so much to surface melt (Holland et al., 2008; Pritchard et al., 2009). For this reason we will take the calving rate, when found to increase slowly, to grow with a constant factor in basal melt projections below.

The basal melt rate is tightly coupled to the local temperature, and in absolute terms to the extent of the ice sheet. When the adjoining ice sheet collapses, the amplitude of the ice discharge goes up tremendously, but the basal melt cannot be expected to follow. Therefore, we can only attribute a certain fraction of D to B as long as the ice sheet is in place (and its surface area is unchanging). After a collapse, or even for a non-linear increase in ice discharge (which will not scale exponentially after a collapse if linked to temperature), the basal melt needs to be re-evaluated. We suggest to set it to zero if a very non-linear event occurs, or allow for a linear increase afterwards (cf. the WAIS in Section 3.2.1).

Here, we provide a description of a set of projections of ice sheet mass loss which follow a high-end scenario of ice loss from the Greenland and Antarctic ice sheets (Katsman et al., 2011), to be used in conjunction with a Representative Concentration Pathway, RCP8.5 scenario (Taylor et al., 2012). For other RCP scenarios that involve ice mass loss can be used by adjusting the appropriate scaling.

Table 2
Overview of melt ratios μ for the Antarctic and Greenland scaling regions.

	Greenland			Antarctica		
	n_i	n_{ii}	n_{iii}	s_i	s_{ii}	s_{iii}
μ	0	0.25	0.25	0.30	0.15	0.40

Table 3
Some conversion factors for the density of (fresh) water at 0 °C and 1 atm. For example, a 1 Sv sustained run-off over the course of a year is equivalent to a global mean sea-level rise of 87.4 mm.

	Gt/yr	mm/yr	Sv
Gt/yr	1	360	$3.15 \cdot 10^4$
mm/yr	$2.78 \cdot 10^{-3}$	1	87.4
Sv	$3.17 \cdot 10^{-5}$	0.0114	1

3.1. Greenland

Greenland is at risk to experience both increased surface melt and glacier retreat (Katsman et al., 2008). The latter is particularly relevant for the Jakobshavn glacier which has already shown considerable retreat (Holland et al., 2008). The processes at work are assumed being the same for the glaciers in region i, and continue to linearly increase the retreat rate during the coming century. As a result, by the year 2100 the rate has been estimated to be four times the current value (Katsman et al., 2011). In region ii, the same progression is assumed, but a retreat to above the waterline is expected by 2050, after which the mass loss rate returns to 1996 values (Rignot, 2006).

The increased global mean temperature is enhanced by local feedback processes with a factor 1.6 (Gregory and Huybrechts, 2006), leading to a greater susceptibility of overall melt and enhanced iceberg calving in region iii. The effect is assumed to cause an increase of sea-level rise, which scales linearly with the local temperature increase (Katsman et al., 2011).

3.1.1. Projection of run-off R

Ice cap run-off is expected to increase linearly with time. Greenland's contribution is expected to be largest of all regions experiencing melt, because its ice mass is more prone to melt due to its location and the temperature feedback with the surrounding ocean (Katsman et al., 2011).

The IPCC's AR5 (Church et al., 2013) (see their Table 13.5, the RCP8.5 scenario) provides a high-end upper limit estimate of 0.13 m sea-level rise caused by the decrease of Greenland's surface mass balance (SMB). Pfeffer et al. (2008) estimate that Greenland's SMB can provide 71 mm and Antarctica 10 mm of sea-level rise. The glaciers and ice caps not associated with these two regions are expected to yield 80 mm. Currently, only Greenland's SMB is lessening (Bamber et al.; Shepherd et al., 2012).

Greenland run-off is given by Bamber et al. as 416 Gt/yr ≅ 0.013 Sv. Fig. 13.9 in the AR5 (Church et al., 2013) indicates that R is expected to increase. If we assume a linear melt rate increase (during the 21st century), we obtain $1.3 \cdot 10^{-2}$ mm/yr^2, or a time-dependent rate of (converted with Table 3)

$$R(t) = 0.013 + (2.96 \cdot 10^{-4} \cdot t)\ \text{Sv} \quad (1)$$

for Greenland's run-off R. The variable t is the number of years since 2000. Run-off is a forcing to be applied to (Greenland's) coastal

grid-cells in the model used. A simulation of Greenland's run-off also shows a linear progression (Mernild and Liston, 2012). The projection of R is shown in Fig. 2. The value of 0.013 Sv is assumed to be the value appropriate for hydrological balance and does not contribute to any rise in sea-level.

3.1.2. Projection of discharge D

Here we give prescriptions for ice discharge in the scaling regions that we distinguish. The initial rate is presumed to be balanced before the epoch ($t \equiv 0$), while the excess value forms the additional imbalance. The initial rate is model-specific, we will address this issue below in A.2. The time index t is to be the number of years since 2000 in all expressions that follow.

Greenland i. The northern glaciers and—in particular—Jakobshavn Isbræ are expected to show a fourfold increase in their rate of the retreat by 2100 (Katsman et al., 2011). Their behaviour is the same in the east and south (see below), except that these termini are not expected to retreat to above sea-level and in the north retreat does not stop during the 21st century. A fraction of 0.18 of the current mass loss is allocated to these regions on the basis of recent mass loss values (see Rignot and Kanagaratnam, 2006 for an overview for Greenland glacial mass loss),

$$D_{n_i}(t) = 69.5 \cdot \left[\frac{3}{104}(t+4)+1\right] \text{ Gt/yr}. \tag{2}$$

The total sea level rise is 10 cm by 2100.

Greenland ii. A doubling of the rate of retreat of the eastern and southern tide-water glaciers by 2050 followed by a return to the balanced rates of 1996 (with 0.21 the fraction of 1996 mass loss, see Table 1) gives,

$$D_{n_{ii}}(t) = 81.7 \cdot \begin{cases} 1/54 \cdot (t+4)+1 & t \leqslant 50 \\ 1 & t > 50 \end{cases} \text{ Gt/yr}. \tag{3}$$

Greenland iii. We use the updated values from IPCC's fifth assessment report (Church et al., 2013), instead of the fourth (Meehl et al., 2007) which was used in Katsman et al. (2008) and Katsman et al. (2011).

An increase of Greenland's discharge D (without the two tide-water glacier areas discussed above) by 2100 is expected due to enhanced run-off caused by a 4 K global-mean atmospheric temperature rise Katsman et al., 2008. The effect is assumed to give an increase of sea-level rise of 0.21 mm/yr for each degree the local temperature increases; this was the increase observed during the period 1993–2003 (Katsman et al., 2011). If we assume that R and D contribute equally to this rise, we find a value of 0.1 mm/yr steady rise in 2000 and 0.32 (=1/2 × 0.4 mm/yr/K × 1.6 global temperature rise increase) additional rise due to increasing temperature. Here the value 0.4 mm/yr/K is given in Katsman et al. (2008) as the mass balance sensitivity with respect to local temperature, the adjustment factor relates this again to global mean temperatures. We find $4/100 \times 0.32 \cdot t$ mm/yr for a linear increase in local Greenland temperature, or (with Table 3)

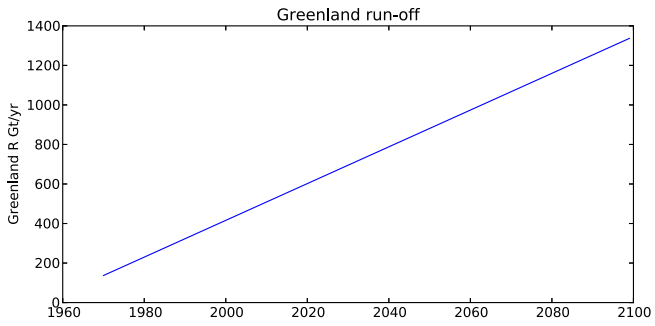

Fig. 2. Mass loss for Greenland run-off (R).

$$D_{n_{iii}}(t) = 36 + (4/100 \times 115 \cdot t) \text{ Gt/yr}. \tag{4}$$

The scaling functions for each of the above three regions are shown in Fig. 3.

3.1.3. Prescription of near-deposition N

The near-deposition of freshwater comprises the melt run-off R and the basal melt rate $\mu \cdot r_n$. The basal melt is location dependent. So far we have collected Jakobshavn and the northern tidewater glaciers together on the basis of the similar processes at work. Measurements of thinning rates indicate that not all of Greenland's glaciers show basal melt Thomas et al., 2006. We should then split up region i into Jakobshavn which does feature basal melt and the northern tidewater glaciers that do not. We label the two ia and i\a respectively. From Table 1 we see that Jakobshavn had a discharge of 27 Gt in 1996, leaving 42.5 Gt for the remaining glaciers. The expressions become

$$N_{n_{ia}}(t) = 27 \cdot \mu_i \cdot \left[\frac{3}{104}(t+4)+1\right] \text{ Gt/yr}, \tag{5}$$

where $\mu_i = 0.25$ for Jakobshavn and

$$N_{n_{i\backslash a}}(t) = 0 \tag{6}$$

for the northern glaciers' N (which is the value given in Table 2 before we made an exception of Jakobshavn). The expressions for the near-depositions in the other two regions have the same numerical value for the basal melt fraction ($\mu_W = \mu_E = 0.25$, where the subscripts indicate west and east, respectively) and can be directly expressed in terms of the ice discharge rate, which leads to

$$N_{n_{ii}}(t) = \mu_{ii} \cdot r_{n_{ii}}(t) \tag{7}$$

for the south/eastern region (ii) and

$$N_{n_{iii}}(t) = \mu_{iii} \cdot r_{n_{iii}}(t) \tag{8}$$

for the third region.

3.1.4. Prescription of far-deposition F

The amount of ice calved and not melted at the base is allowed to drift. This is the amount that we will distribute according to the pattern produced by the iceberg drift simulation detailed below in A.1. Taking the split of region i into account we have

$$F_{n_{ia}}(t) = 27 \cdot (1-\mu_W) \cdot \left[\frac{3}{104}(t+4)+1\right] \text{ Gt/yr} \tag{9}$$

for Jakobshavn's F and

$$F_{n_{i\backslash a}}(t) = 42.5/69.5 \cdot r_{n_i}(t) = 42.5 \cdot \left[\frac{3}{104}(t+4)+1\right] \text{ Gt/yr} \tag{10}$$

for the northern glaciers' F. Here, we have assumed μ to remain constant throughout time, effectively allowing the melt amount to

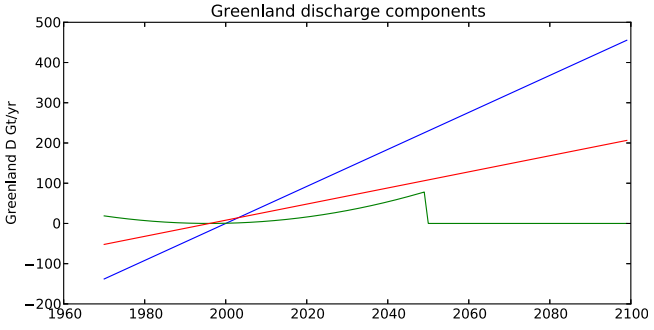

Fig. 3. Scaling functions of the components of ice discharge (D) for Greenland. In blue D_{n_i}, green $D_{n_{ii}}$, red $D_{n_{iii}}$.

scale with the ice discharge rate. Because the rate changes only linearly, this is not an unreasonable assumption. We merely assume that a larger ice mass is present when D increases. In the case of Antarctica (see below), this assumption breaks down when collapsing ice sheets need to be taken into account.

3.2. Antarctica

The high-end scenario we use Katsman et al., 2008 includes an accelerated outflow of the Amundsen Sea Embayment, with a collapse in the year 2030 after which the loss rate remains constant at eight times the current value. The loss is assumed to increase exponentially up to the break-point. A similar progression is assumed to hold for the glaciers in east Antarctica, except that the difference in grounding prevents a retreat as advanced as for the ASE. After 2030 the mass loss increases with a greater exponential rate. The Peninsula region is assumed to experience enhanced melt and glacier flow with a similar progression as the EAIS region, but the quantity is much less.

3.2.1. Projection of discharge D

A projection to match the storylines involves constructing a parametrisation of the loss rate. To be able to do so the current loss rates are required.

Antarctica i. The severe scenario includes a collapse of the west-Antarctic ice shelf, the inclusion of which is based on expert judgment (Katsman et al., 2011). The collapse of the Larsen-B ice shelf has shown such an event to cause an increase of 2–6× the speed of the shelf's feeding glaciers (Scambos et al.). If we assume this speed-up factor to also hold for the WAIS with respect to current feeding rates, a total sea-level rise in the order of 0.25 m by 2100 is expected (Katsman et al., 2011). The storyline assumes that by 2030 a 50% excess discharge has taken place and the collapse is initiated. The removal of the ice shelf increases (near instantaneously) the calving rate by a factor 8 of the balanced discharge value.[2] This positive feedback causes the glaciers to calve at an exponential rate. With a 237 Gt/yr of outflow calving and 177 of input for Pine Island and Twaites glacier—this is also the base-rate added for full ice flux values, taken from Rignot et al. (2008) (their Table 1) and a sustained acceleration of 1.3%/yr,

$$D_{s_i}(t) = 237 + \begin{cases} 237 \cdot \left[(1.013)^t - 1\right] & t \leqslant 30 \\ 177 \times 7 & t > 30 \end{cases} \text{Gt/yr.} \tag{11}$$

Antarctica ii. The eastern glaciers are expected to retreat like those in the western part except that east Antarctica rests on a high plateau. The eastern glaciers are then thought to be less susceptible to collapse Rignot, 2006 because marine glaciers will not be able to retreat so easily. The outflow of ice of the eastern ice sheet is 785 Gt/yr (Rignot et al., 2008) and 388 (=87 + 207 + 94, from Table 1 in Rignot et al. (2008)) Gt/yr is due to the glaciers bounded by the ice sheet (this is the base calving rate). Katsman et al. (2011) assume the same initial storyline as for the western sector. After this period exponential growth is expected. The integrated contribution to sea-level rise by 2100 would be 0.19 m. Under these constraints we find 0.0385 in the exponent for the post-2030 rate,

$$D_{s_{ii}}(t) = 388 + 388 \cdot \begin{cases} (1.013)^t - 1 & t \leqslant 30 \\ \left[(1.013)^{30} - 1\right] \cdot e^{0.0385 \cdot (t-30)} & t > 30 \end{cases} \text{Gt/yr.} \tag{12}$$

[2] Katsman et al. (2011) quote 8 as an upper bound, and 8 = 6 × 237/177, the fraction of the 2000 outflow to the input. The balance value they speak of is the input rate.

Antarctica iii. Assuming an effect of 0.05 m sea-level rise by 2100 (Katsman et al., 2008), with again assuming the same structure of the equation for the region ii, we find 0.0375 for the exponential rate,

$$D_{s_{iii}}(t) = 107 + 107 \cdot \begin{cases} (1.013)^t - 1 & t \leqslant 30 \\ \left[(1.013)^{30} - 1\right] \cdot e^{0.0375 \cdot (t-30)} & t > 30 \end{cases} \text{Gt/yr.} \tag{13}$$

The scaling functions for the discharge amount associated with each of the above three regions are shown in Fig. 4.

The combined discharge rates are shown in Fig. 5. An accumulation-balancing rate of 107 Gt/yr is given by Rignot et al. (2008). The effect of increased snow accumulation on Antarctica during the immediate future (as indicated by observations Church et al., 2013) would mean a larger potential value for D. Measurements from Rignot and Kanagaratnam (2006) and Rignot et al. (2008) are shown as well in Fig. 5. More recent overviews (Shepherd and Wingham, 2007; Shepherd et al., 2012) show considerable variation in the Greenland and Antarctic mass balance measurements. Because the sampling was performed during different periods and does not include all ice sheets, we have left these from further consideration.

3.2.2. Prescription of near-deposition N

The progression of D in Fig. 4 shows the collapse of the West-Antarctic ice sheet. The discharge rate increases dramatically with this event. With the ice sheet gone, calved icebergs drift more easily. We expect basal melt to decrease then. On the other hand, more land ice is in contact with the ocean, which should increase the absolute amount of melt taking place. Without any way of quantifying either effect, we suggest that after a collapse event the basal melt amount returns to pre-collapse levels. The expression becomes

$$N_{s_i}(t) = \begin{cases} \mu_i \cdot D_{s_i}(t) & t \leqslant 30 \\ \mu_i \cdot D_{s_i}(30) & t > 30 \end{cases} \text{Gt/yr} \tag{14}$$

for the WAIS (region i), where $\mu_W = 0.30$. Similar considerations to those above lead us to keep the amount of basal melt steady at the 2030 levels for the other two regions, which then give the exact same form as Eq. (14) with the appropriate μ values (Table 2).

3.2.3. Prescription of far-deposition F

Far deposition is allocated to all mass loss not already claimed by basal melt. The expression for Antarctic F is then simply

$$F_s(t) = \begin{cases} (1 - \mu_s) \cdot D_s(t) & t \leqslant 30 \\ D_s(t) - (\mu_s \cdot D_s(30)) & t > 30 \end{cases} \text{Gt/yr.} \tag{15}$$

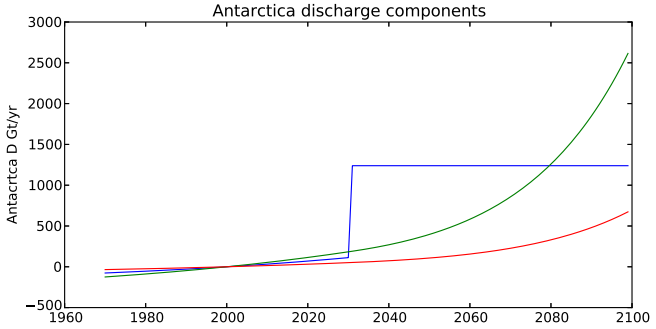

Fig. 4. Scaling functions of the components of ice discharge (D) for Antarctica. In blue D_{s_i}, green $D_{s_{ii}}$, red $D_{s_{iii}}$.

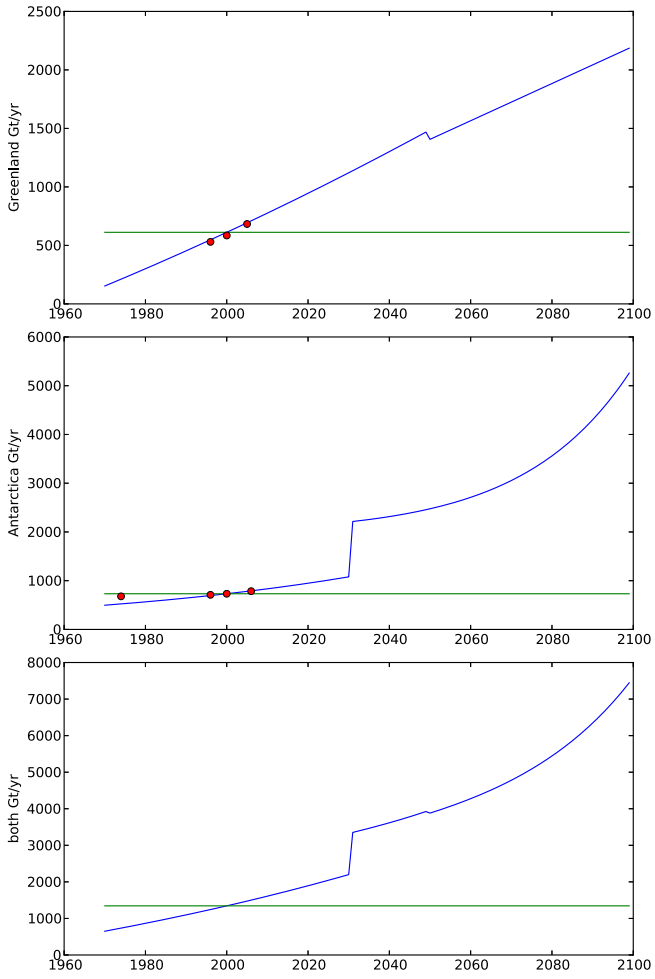

Fig. 5. Mass loss for Greenland, Antarctica and their sum. The horizontal lines show the equilibrium values. Some measurements are shown as well. These were taken from Rignot et al. (2008) for Antarctica and from Rignot and Kanagaratnam (2006) for Greenland. The Greenland values were obtained by assuming the mass balance differences are entirely attributable to ice discharge changes in regions i and ii. Uncertainties in the original measurements are $\sim 10\%$.

for all three regions with μ_s replaced by the appropriate basal melt fraction and r_s the corresponding discharge rate.

Table 4 gives a summary of the melt scenario features on which our projections are based.

3.3. Comparison with other projections

In Table 5 a break-down of mass loss expressed as sea-level equivalent is given. We can compare with some other severe scenarios, see Fig. 6. The most recent scenarios are by Pfeffer et al. (2008) and Katsman et al. (2011). A projection close to the values given by Pfeffer et al. (2008) as upper bounds would tax the rate of retreat of the tidewater glacier to nonphysical limits. The lower bound from Fettweis et al. (2013) only takes meltwater into account. The projections for ice discharge dominate this by an order of magnitude.

4. Effect on the sea-surface

To illustrate the effect of the freshwater protocol outlined above, we ran a RCP8.5 experiment with the CCM EC-Earth (Hazeleger et al., 2010). One simulation was run without the extra freshwater forcing applied (*control*) and one with additional freshwater forcing included (*forced*) to allow for a sensitivity experiment. The control run is part of the CMIP5 archive and both runs use the RCP8.5 forcing a described in Taylor et al. (2012).

We expect the additional freshwater to immediately affect local sea-surface height and through barotropic effects to propagate information throughout the world ocean (Stammer et al., 2011; Lorbacher et al.). The freshwater might also affect ocean currents.

In the forced run the North Atlantic sub-polar gyre remains weakly affected for a considerable time. It is not until 2075 that the mean sea-level rise is comparable to the local rise in the gyre (not shown). The reason for this is that most of added the freshwater is taken away by boundary currents in the Northern Hemisphere. The same can be seen in other experiments of comparable resolution with Greenland freshwater release like (Stammer et al., 2011; Kopp et al., 2010; Weijer et al.; Swingedouw et al., 2013).

A climate model is a chaotic system and shows sensitivity to small variations in initial conditions. An ensemble of runs can bring out the so called internal variability. We have used such an ensemble of control runs to determine the variance in the SSH. In Fig. 7 the areas where the rise does not exceed 2σ are mapped onto the eustatic sea-level, where the whitepoint is centred. The model allows for a free-surface adjustment which shows an increase of SSH with the addition of more freshwater as can be seen in the lower panel.

The response to the freshwater forcing is largely advective with the mean subpolar gyre circulation transporting the melt water southward. This can be seen by the comma-shaped feature present in both panels and lying more to the east in the lower one. To the west and south of the sub-polar gyre the sea-surface anomaly is larger than within the gyre, or to the north. The west-to-east gradient in the North Atlantic with a strong anomaly along the north-east coast of North America, as noted in Kopp et al. (2010), can also be seen in the top panel of Fig. 7.

The lower panel, which depicts the situation for the last five years of the century, shows an opposite pattern. Here, a positive anomaly on the eastern side of the Atlantic basin can be seen. The formation/inversion of this pattern is also present in the atmosphere-coupled run discussed in Stammer et al. (2011). A strong signal develops along the American coast and a signal similar to the one in the lower panel of Fig. 7 can be seen after four decades (see also Swingedouw et al., 2013 for a comparison between several models showing a similar pattern).

The additional freshwater does not impact the Atlantic meridional overturning. In Fig. 8 the annual mean of its maximum value is shown for the RCP8.5 only run (green) and with the freshwater added (blue). The difference (red) indicates little difference between the two. The maximum mixed layer depth (not shown) shows some decrease in the Labrador region and an increase north of Iceland, but this effect is highly variable. We surmise that most of the freshwater does not reach the convection regions and has little impact on dense-water formation. We cannot ascertain whether spatial changes occur as a result of this (i.e. the possible shifting north of the convection regions).

The signal in the eastern North Atlantic is described in Swingedouw et al. (2013) where the authors show that the leakage (i.e. removal of freshwater that then does not re-circulate) relates to the meridional tilt of the separation between the sub-polar and the sub-tropical gyre. The leakage via the Canary current (the eastern branch of the pattern) diminished the amount of freshwater that is transported to the convection sites in the Labrador Sea and Nordic Seas and could then affect the intensity of deep convection if the leakage is sufficiently large. This also occurs in EC-Earth.

The long-term pattern of freshwater in our forcing field as shown in Fig. 7 resembles the observed anomaly in sea-level rise

Table 4
Summary of the melt scenario characteristics. Details are given in the text and figures.

	Region	Now	Future
SMB	Greenland	416 Gt/yr	Linear increase
Calving	Northern tw. glaciers (i)	69.5 Gt/yr	"
	Eastern/southern tw. glaciers (ii)	81.7 Gt/yr	Linear increase until 2050, then return to current value
	Other glaciers (iii)	36 Gt/yr	Linear increase
Basal melt	Northern tw. glaciers (i)	0	0
	Eastern/southern tw. glaciers (ii)	0.25	Scale with calving rate
	Other glaciers (iii)	0.25	"
SMB	Antarctica	In equilibrium	Unchanged
Calving	WAIS (i)	237 Gt/yr	Acceleration until 2030, then kept constant
	EAIS (ii)	388 Gt/yr	Acceleration until 2030, then mild exponential increase
	N-AP (iii)	107 Gt/yr	"
Basal melt	WAIS (i)	0.30	Scale with calving rate until 2030, then kept constant
	EAIS (ii)	0.15	"
	N-AP (iii)	0.40	"

Table 5
Comparison of sea-level equivalent rise (mm) per contributor region for a selection of years. Discrepancies in the added numbers are due to round-off error. Columns 6 and 10 are the sums of columns 2–5 and 7–9, respectively.

	Greenland (mm)					Antarctica (mm)			
	R	D_i	D_{ii}	D_{iii}		D_i	D_{ii}	D_{iii}	
2000	0	0	0	0	0	0	0	0	0
2005	0.32	0.16	0.14	0.18	0.80	0.11	0.18	0.049	0.34
2020	5.2	2.6	1.2	1.6	11	1.9	30	0.84	33
2030	11.6	5.8	2.4	3.2	23	4.4	7.2	2.0	14
2050	32	16	6.0	8.1	62	73	23	6.2	102
2100	130	64	6.0	30	230	245	190	50	485

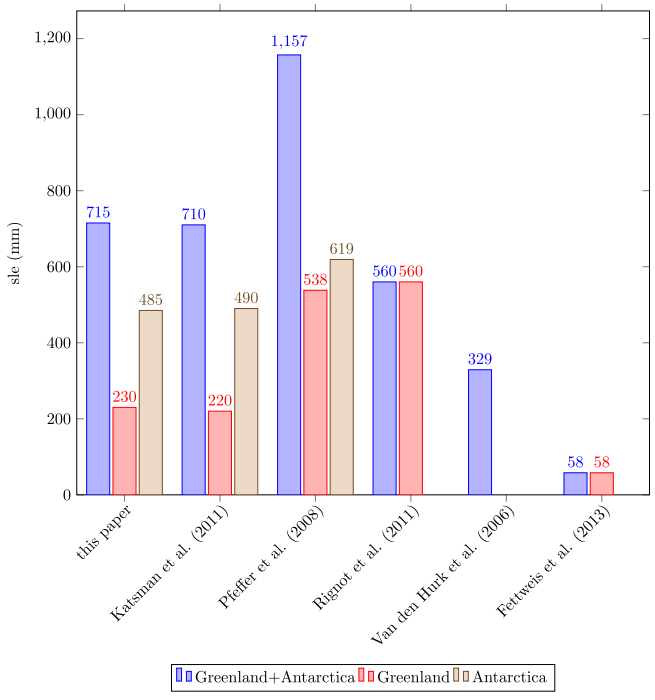

Fig. 6. Histogram comparison of different mass loss projections. The cited sources are Katsman et al. (2011), Pfeffer et al. (2008), Rignot et al. (2011), van den Hurk et al. (2007) and Fettweis et al. (2013).

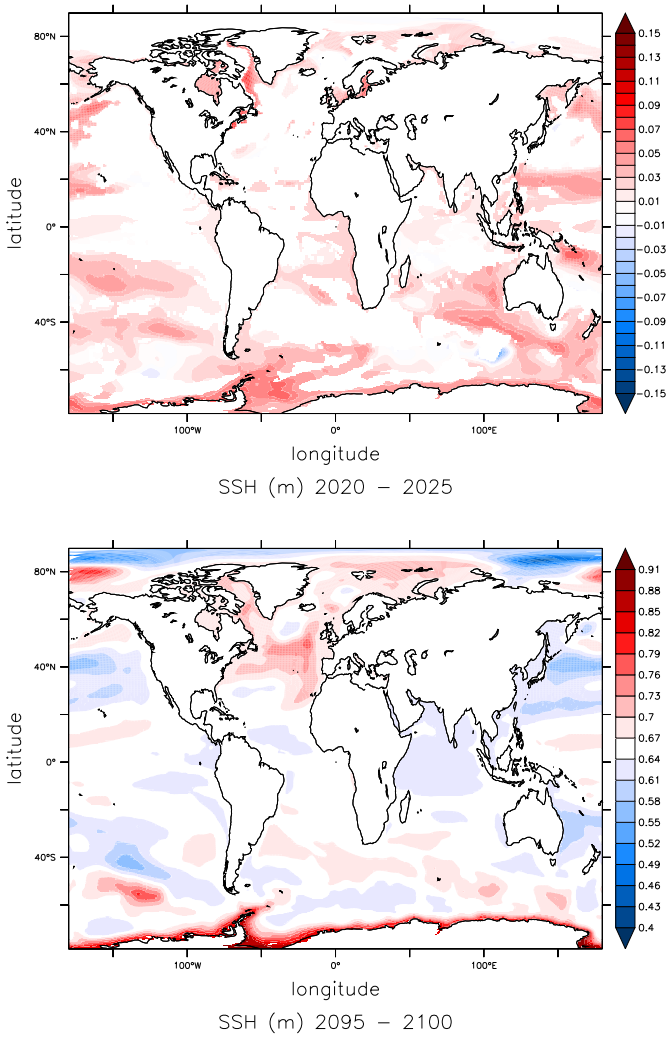

Fig. 7. Top panel: sea-surface height anomalies of 5-year averages for the indicated period. Lower panel: the situation in 2095 (the whitepoint corresponds to the eustatic sea-level rise). The Arctic consistently lags behind the rest of the ocean in rise. Non-significant rises (at the 2σ level with respect to an ensemble of RCP8.5 forced control runs) are mapped onto the eustatic level, the whitepoint.

near the Antarctic ice shelves shown in Fig. 1 in Rye et al. (2014). The only conspicuous difference is that we have a somewhat larger melt in the northern peninsula region. The gross Antarctic sea-level rise pattern in Rye et al. (2014) is also present in our simulation. In the Southern Hemisphere, the freshwater released along the coast

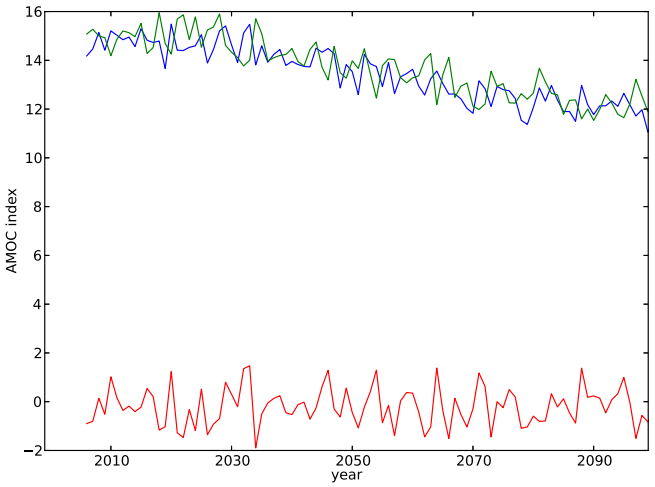

Fig. 8. The maximum of the annually averaged Atlantic meridional overturning circulation. Blue shows the run with freshwater forcing, green without, and red the difference between the two.

of Antarctica spreads northward and is thereafter taken up by the Antarctic Circumpolar Current (ACC), spreading it in a band around Antarctica. The same pattern around Antarctica can be seen in the simulation described in Lorbacher et al., where the fast response to Antarctic melt occurs on a timescale of mere days. This is remarkable because the fast response is due to barotropic waves and not directly related to the long-term response. In Fig. 3 in Rye et al. (2014) the sea-level rise in a model output indicates locally larger relative rise than is in our simulation.

5. Discussion

Recent experiments with high resolution, eddy-resolving, models (Weijer et al.; Spence et al., 2013; den Toom et al., 2014) indicate qualitative differences in large-scale circulation compared with coarse-resolution ones ($\sim 1^\circ$) like EC-Earth. The circulation shows different ventilation pathways (Spence et al., 2013) of North Atlantic Deep Water (NADW), which is not surprising given the finer topography and different diffusion value needed. Also, deep convection regions persist longer at higher resolution (Weijer et al.; Spence et al., 2013). The entrainment along the western boundary lasts longer compared to a low-resolution model which favours a more immediate transport to the deep convection zones (Spence et al., 2013). The short-term response in a high-resolution model can be different, but this does not necessarily mean a significant difference in behaviour on decadal timescales (Weijer et al.). Caveats like these suggest that a significant improvement in realism can be expected when high-resolution models are coupled with atmospheric models (den Toom et al., 2014), which has not been feasible so far.

Nevertheless, our run does show similarities with higher-resolution (den Toom et al., 2014). We can compare with the results of another freshwater forcing experiment in the same vein, which indicates only little impact on the large-scale circulation (Marsh et al., 2010). There, the additional freshwater accumulates west of Greenland and leaves the subpolar gyre largely unaffected. The same effect is seen in our simulation (Fig. 7).

Ice mass loss like in our scenario does not lead to significant decrease in the height of the ice sheet. We therefore do not expect any changes in the feedbacks between the ice sheet and the atmosphere. Since retreat of glaciers does affect the interaction with the ocean (at least locally), some feedbacks will be affected by ice melt. We try to account for one of these, basal melt, but a detailed treatment requires more advanced modelling.

Climate scenarios contain a lot of uncertain elements. Such scenarios are also subject to change. By being a precise as possible we hope to accommodate future scenarios.

6. Summary

We have presented a simple, yet flexible way to apply a patterned freshwater forcing to the ocean surface based on realistic, yet high-end, Greenland and Antarctica mass loss scenarios. The projection of run-off (R), basal melt (B), and ice discharge (D) in excess of balanced values—which have not been met in Greenland for the past twenty years—show an increase in the calving rates of both the Antarctic and Greenland glaciers. The final contributions of excess production of R, B and D remain within the maximum bounds determined by Pfeffer et al. (2008). In the scenario we used, it was assumed that a collapse of the West Antarctic ice sheet occurs, which will accelerate mass loss tremendously before mid-century. The total mass loss from the two large ice sheets becomes dominated by the ice discharge contribution.

The sea-surface height in the sub-polar gyre in the North Atlantic is affected only little, with a smaller than average increase throughout the 21st century. The area around Antarctica sees a steady increase on the other hand, and maximal values can be found there. This is due to the large forcing in the region associated with iceberg calving in the scenario.

The protocol we have proposed aims to provide an affordable way to extent the current numerical models to deal with melting ice sheets. Effects like a realistic spatial pattern of freshwater accumulation are encouraging.

Acknowledgements

Thanks go out to Wilco Hazeleger, Roderik van de Wal, Camiel Severijns, and especially Caroline Katsman, for useful comments and suggestions. The authors also thank Bob Marsh and Vladimir Ivchenko for contributing their iceberg simulation. We would also like to thank our three anonymous referees for their suggestions and comments. This work was funded by the European Commission's 7th Framework Programme, under Grant Agreement number 282672, EMBRACE project.

Appendix A. Implementation

In the previous sections we developed a description for time-series of location-dependent freshwater forcing, derived from projections of meltwater run-off (R), basal melt (B), and iceberg calving (D). Because these quantities are either applied to a location near the source or further away from it, we constructed the N and F prescriptions. The scaling regions' mass loss can be scaled independently according to the above scenarios. To implement the projections we have to account for any freshwater forcing already applied in the model. Most climate models balance snow accumulation on Greenland and Antarctica with a prescribed run-off. We propose to start at time zero (year 2000) with a freshwater flux that balances the already prescribed flux in the model, only changing the spatial distribution. Afterward we allow for a growing imbalance between snow accumulation and freshwater gain according to our melt projections.

A.1. Iceberg drift

The far deposition F of freshwater forcing needs a prescribed annual pattern. Output of a simulation of iceberg drift provides this pattern and the amount of melt loss. The amount of meltwater from icebergs was determined at every cell on the grid of a

$2^\circ \times 2^\circ$ ocean model (Madec, 2008). The pattern thus obtained is an annual one. We subdivide the iceberg pattern in a Northern and a Southern Hemispheric region. We assume that all freshwater flux found north of the equator is attributable to Greenland mass loss and likewise all found south of the equator is attributable to Antarctic sources. Because the forcing pattern (Fig. A.9) alone does not contain any information about the original source of icebergs, the scaling of the far-deposition F can only be applied per hemisphere.

The basal melt pattern only varies within a single year, meaning we can scale the seven region-dependent contributions of N according to their individual annual prescription.

The spatial pattern of freshwater forcing from iceberg melting is obtained from the output of an iceberg tracking simulation. Because only the pattern is of interest (the total amount of mass loss due to icebergs is normalised), we do not need to re-grid the iceberg melt in a strictly conservative way, but only approximately. Instead we simply locate the original grid-cell nearest to a target grid-cell and use the value it has (we do scale with the area of each grid-cell).

A.2. Scaling and distribution

Our starting point is maintaining (approximate) continuity with historical conditions. We demand that our scenarios for $t = 0$ (year 2000) have equal amounts of freshwater forcing as the total of prescribed run-off around Greenland and Antarctica in the model forcing. We note that the observational estimates for present day mass loss (in our scenarios the value at $t = 0$) may differ from the model's total sum. When replacing these, we maintain the relative ratios for basal melt, iceberg calving and run-off obtained from the observations, but re-scale the total observed mass loss to match the total in the model. The relative contributions in the scenario projections are given in Table A.6.

A.2.1. Run-off

In our scenario only Greenland experiences run-off. This will be distributed equally along Greenland's coastal grid-cells, a single cell wide. Any Antarctic run-off would be negligible with respect to other melt loss processes, since a mass increase seems more likely (Church et al., 2013).

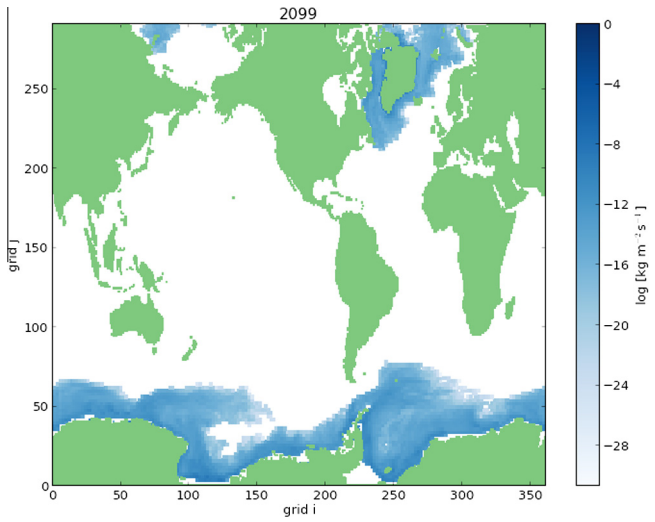

Fig. A.9. Annual average of the iceberg pattern used to distribute the far deposition F of freshwater forcing amount in EC-Earth. Darker blue indicates a greater relative amount is deposited.

A.2.2. Iceberg melt flux

We cannot distinguish the origin of icebergs any finer than from which hemisphere they originate. We simply sum the far deposition for north and south and scale the iceberg melt flux in each half of the globe,

$$F_n(t) = F_{n_{\mathrm{ia}}}(t) + F_{n_{\mathrm{ia}}}(t) + F_{n_{\mathrm{ii}}}(t) + F_{n_{\mathrm{iii}}}(t) \quad (A.1)$$

$$F_s(t) = F_{s_{\mathrm{i}}}(t) + F_{s_{\mathrm{ii}}}(t) + F_{s_{\mathrm{iii}}}(t). \quad (A.2)$$

The fractions listed in Table A.6 provide the relative weights that each region should have. In the final expressions for F, the initial values reported in Section 4 are replaced with the fractions of total mass loss due to ice discharge specific to the model.

A.2.3. Basal melt deposition

To provide a correct deposition of the basal melt freshwater we need to take the relative strength of discharge into account. We take the values for the ice discharge as presented in Rignot and Kanagaratnam (2006) for Greenland and assign the locations given to the nearest grid-cell in a mask of the grid layout as used in our model. Masks are then made for the relevant Greenland and Antarctic regions, so that we are able to independently control the melt intensity of each.

For each region a collection of point sources is defined to determine the basal melt freshwater release location in Fig. A.10. In the case of a glacier this would be a single point, in a region such as the North-Antarctic Peninsula several points. By associating an area of deposition (set to a default of 2000 km^2 for each point source) with each source, we can enumerate the nearest grid-cells and subtract their area until exhaustion of the deposition area. We use the Euclidean distance to weigh the relative amount of meltwater that is to be deposited in each grid-cell. A cell nearer to the source receives more mass. The point sources and associated variable values are given in Table B.7 for Greenland and in Table B.8 for Antarctica. In this way a zone of deposition can be defined. The basal melt pattern consists of six regional contributions, each with an independent scaling (scaling region).

In addition, we wish to take the presence of sills into account because they might act as a barrier and trap water. For each grid-cell that is enumerated, we define the line of grid-cells between it and the source cell (a linear equation of the latitude/longitude coordinates). We then attempt to locate the sill as the barrier nearest to the source. A barrier is defined as an ocean grid-cell where the depth is less than the depth associated with the cell closer to the source in the line, effectively a bump in the bottom topography. All grid-cells belonging to the line before the sill are used as the deposition area. The typical number of cells per point source is one or only a few grid-cells for a $1^\circ \times 1^\circ$ grid.

A.3. Seasonality

Surface melt does not occur throughout the year, but tends to be limited to summer. We model this restriction with a seasonality function, for which we assume a step distribution σ. For the North-

Table A.6
The initial (r_0) run-off and ice discharge values (in Gt/yr, total of 1274.54 Gt/yr) and their fractional share of the Antarctic or Greenland part (or hemispheric share). The total initial amount of freshwater forcing should be kept the same at time = 0 to ensure hydrological balance in the model.

	Greenland				Antarctica		
	$D_{n_{\mathrm{i}}}$	$D_{n_{\mathrm{ii}}}$	$D_{n_{\mathrm{iii}}}$	R	$D_{s_{\mathrm{i}}}$	$D_{s_{\mathrm{ii}}}$	$D_{s_{\mathrm{iii}}}$
Amount (Gt/yr)	69.5	81.7	36	416	177	388	107
Fraction	0.69	0.12	0.14	0.06	0.26	0.58	0.168

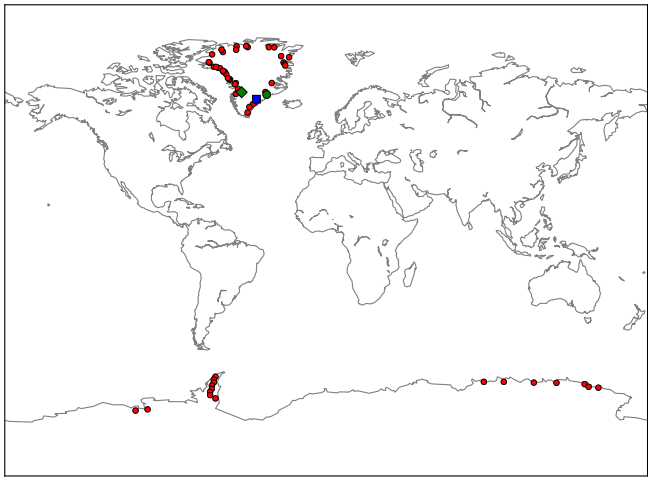

Fig. A.10. Points used to determine mass deposition areas. Indicated with a green diamond is Jakobshavn, with a blue square Kangerdlugssuaq, and with a green circle Helheim. Actual freshwater fluxes (e.g. run-off) are not shown.

ern Hemisphere we take summer to start in May, ending in September, and for the Southern Hemisphere beginning in November, ending in March. We correct for this by scaling annual values with a factor 2.4 (=12/5) during summer. During summer the function is 'on' and otherwise 'off',

$$\sigma(t) = \begin{cases} 2.4 & \text{summer}(t) \\ 0 & \text{winter}(t). \end{cases} \tag{A.3}$$

The seasonality function must be multiplied with N. Care must be taken that the total amount of mass loss in a year remains the same as in the original prescription.

A.4. Synthesis

The final product is a time-series of freshwater forcing per grid-cell. No explicit reference during run time of the simulation is needed to the various expressions and regions we have distinguished here. All grid-cells where no value is defined receive a value of 0, and all separately scaled contributions are summed to a single time-dependent pattern. This time-series can now be used as a forcing field to mimic a realistic freshwater forcing as the result of, not only meltwater, but also iceberg calving and the basal melt associated with them. The recipe consists of the following steps.

1. remove the existing freshwater forcing associated with Greenland and Antarctica;
2. set the r_0 values to match the loss in any previous freshwater forcing to maintain balance;
3. for each region in Greenland and Antarctica: mask region and multiply with the projection value;
4. for the Northern and Southern Hemisphere: sum the projections in each (according to Eqs. (A.1) and (A.2)) and scale the hemispheric pattern with this sum; the forcing is applied to the surface as additional water with local temperature;
5. apply the sum of the series as a freshwater forcing to the ocean model.

Appendix B. Mass loss point sources

See Tables B.7 and B.8.

Table B.7
Point sources used to define the basal melt regions in Antarctica. Several points can belong to a single glacier if it is extended over a large area. The area is the surface in km^2. The discharge values were taken from Rignot and Kanagaratnam (2006).

Region	Position (ϕ, λ)	Size (km^2)	D (Gt/yr)	Name
$D_{n_{ia}}$	(68.9, −47.3)	8000	27	Jakobshavn Isbræ
	(69.1, −49.4)			
	(69.2, −48.2)			
	(69.2, −47.7)			
$D_{n_{ii}}$	(77.6, −23.9)	6000	6.8	Storstrømmen
	(77.2, −23.2)			
	(76.8, −22.9)			
	(71.8, −30.5)	2000	10.5	Daugaard-Jensen
	(68.2, −33.3)	4000	27.9	Kangerdlugssuaq
	(69.0, −34.0)			
	(66.7, −39.0)	4000	26.2	Helheim
	(66.4, −38.4)			
	(65.5, −39.7)	2000	10.3	Ikertivaq
$D_{n_{iii}}$	(65, −41)	6000	67.4	
	(64, −43)			
	(62, −44)			
	(68.4, −50.6)	2000	10.7	Nordenskiold
	(70.0, −49.3)	2000	10.9	Sermeq Kujatdleq
	(71.5, −51.1)	2000	2.7	Kangerdlugssup
	(71.8, −50.6)	2000	12.1	Rinks
	(72.8, −53.8)	4000	8.6	Upernavik
	(73.0, −54.4)			
	(73.3, −55.0)	2000	4.7	Nunatakavasaup
	(74.4, −56.0)	2000	7.1	Igdlugdlip
	(74.9, −56.7)	6000	10.9	Hayes
	(75.0, −56.8)			
	(75.0, −57.4)			
	(75.1, −57.6)	4000	1.3	Steenstrup
	(75.4, −57.8)			
	(76.1, −59.5)	2000	8.5	Kong Oscar
	(76.2, −60.5)	2000	8.5	Peary/Docker
	(76.4, −62.9)	2000	3.3	Gades
	(76.4, −61.7)	2000	64.4	

Table B.8
Point sources used to define the basal melt regions. The area is the surface in km^2.

Region	Position (ϕ, λ)	Size (km^2)	D (Gt/yr)	Name
D_{S_i}	(−75.2, −100)	4000	87	WAIS
	(−75.5, −106.7)			
$D_{S_{ii}}$	(−66.8, 88.3)	4000	87	EAIS
	(−66.8. 99.5)			
	(−67, 116.3)	4000	94	
	(−67.1, 129)			
	(−68.7, 152.5)	6000	237	
	(−67.5, 144.8)			
	(−68.4, 147)			
$D_{S_{iii}}$	(−65, −62)	16000	107	N-AP
	(−66, −63)			
	(−67, −63)			
	(−68, −64)			
	(−69, −64)			
	(−70, −65)			
	(−71, −65)			
	(−72, −62)			

References

Alley, R.B., Horgan, H.J., Joughin, I., Cuffey, K.M., Dupont, T.K., Parizek, B.R., Anandakrishnan, S., Bassis, J., 2008. A simple law for ice-shelf calving. Science 322 (5906), 1344. http://dx.doi.org/10.1126/science.1162543.

Amundson, J.M., Truffer, M., 2010. A unifying framework for iceberg-calving models. J. Glaciol. 56 (199), 822–830. http://dx.doi.org/10.3189/002214310794457173.

Bamber, J., van den Broeke, M., Ettema, J., Lenaerts, J., Rignot, E., Recent large increases in freshwater fluxes from Greenland into the North Atlantic. Geophys. Res. Lett. 39 (19). http://dx.doi.org/10.1029/2012GL052552.

Beckmann, A., Goosse, H., 2003. A parameterization of ice shelfocean interaction for climate models. Ocean Modell. 5 (2), 157–170. http://dx.doi.org/10.1016/S1463-5003(02)00019-7.

Bigg, G.R., Wadley, M.R., Stevens, D.P., Johnson, J.A., 1996. Prediction of iceberg trajectories for the north Atlantic and Arctic oceans. Geophys. Res. Lett. 23 (24), 3587–3590. http://dx.doi.org/10.1029/96GL03369.

Bigg, G.R., Wadley, M.R., Stevens, D.P., Johnson, J.A., 1997. Modelling the dynamics and thermodynamics of icebergs. Cold Regions Sci. Technol. 26 (2), 113–135, <http://dx.doi.org/10.1016/S0165-232X(97)00012-8>.

Church, A., Clarck, P., Cazenave, A., Gregory, J., Jevrejeva, S., Levermann, A., Merrifield, M., Milne, G., Nerem, R., Nunn, P., Payne, A., Pfeffer, W., Stammer, D., Unnikrishnan, A., 2013. Sea level change. In: Climate Change 2013: The Physical Science Basis. Contribution of Working Group I to the Fifth Assessment Report of the Intergovernmental Panel on Climate Change. Cambridge University Press.

den Toom, M., Dijkstra, H.A., Weijer, W., Hecht, M.W., Maltrud, M.E., van Sebille, E., 2014. Sensitivity of a strongly eddying global ocean to North Atlantic freshwater perturbations. J. Phys. Oceanogr. 44, 464–481. http://dx.doi.org/10.1175/jpo-d-12-0155.1.

ECMWF, IFS documentation, 2006.

Fettweis, X., Franco, B., Tedesco, M., van Angelen, J.H., Lenaerts, J.T.M., van den Broeke, M.R., Gallée, H., 2013. Estimating the Greenland ice sheet surface mass balance contribution to future sea level rise using the regional atmospheric climate model mar. Cryosphere 7 (2), 469–489. http://dx.doi.org/10.5194/tc-7-469-2013.

Gregory, J.M., Huybrechts, P., 2006. Ice-sheet contributions to future sea-level change. Philos. Trans. R. Soc. A: Math. Phys. Eng. Sci. 364 (1844), 1709–1732. http://dx.doi.org/10.1098/rsta.2006.1796.

Greve, R., Blatter, H., 2009. Dynamics of Ice Sheets and Glaciers. Advances in Geophysical and Environmental Mechanics and Mathematics. Springer-Verlag. http://dx.doi.org/10.1007/978-3-642-03415-2.

Hanna, E., Huybrechts, P., Steffen, K., Cappelen, J., Huff, R., Shuman, C., Irvine-Fynn, T., Wise, S., Griffiths, M., 2008. Increased runoff from melt from the Greenland ice sheet: a response to global warming. J. Clim. 21 (2), 331–341. http://dx.doi.org/10.1175/2007JCLI1964.1.

Hazeleger, W., Severijns, C., Semmler, T., Ştefanescu, S., Yang, S., Wang, X., Wyser, K., Dutra, E., Baldasano, J.M., Bintanja, R., Bougeault, P., Caballero, R., Ekman, A.M.L., Christensen, J.H., van den Hurk, B., Jimenez, P., Jones, C., Kållberg, P., Koenigk, T., McGrath, R., Miranda, P., van Noije, T., Palmer, T., Parodi, J.A., Schmith, T., Selten, F., Storelvmo, T., Sterl, A., Tapamo, H., Vancoppenolle, M., Viterbo, P., Willén, U., 2010. EC-Earth: a seamless earth-system prediction approach in action. Bull. Am. Meteorol. Soc. 91 (10), 1357–1363. http://dx.doi.org/10.1175/2010BAMS2877.1.

Hazeleger, W., Wang, X., Severijns, C., tefnescu, S., Bintanja, R., Sterl, A., Wyser, K., Semmler, T., Yang, S., Hurk, B., Noije, T., Linden, E., Wiel, K., 2012. Ec-Earth v2.2: description and validation of a new seamless earth system prediction model. Clim. Dyn. 39 (11), 2611–2629. http://dx.doi.org/10.1007/s00382-011-1228-5, URL <http://dx.doi.org/10.1007/s00382-011-1228-5>.

Hellmer, H.H., Kauker, F., Timmermann, R., Determann, J., Rae, J., 2012. Twenty-first-century warming of a large Antarctic ice-shelf cavity by a redirected coastal current. Nature 485 (7397), 225–228. http://dx.doi.org/10.1038/nature11064.

Holland, D.M., Thomas, R.H., de Young, B., Ribergaard, M.H., Lyberth, B., 2008. Acceleration of Jakobshavn Isbr triggered by warm subsurface ocean waters. Nat. Geosci. 1 (10), 659–664. http://dx.doi.org/10.1038/ngeo316.

Jenkins, A., Holland, D., Melting of floating ice and sea level rise. Geophys. Res. Lett. 34 (16). http://dx.doi.org/10.1029/2007GL030784.

Katsman, C., Hazeleger, W., Drijfhout, S., Oldenborgh, G., Burgers, G., 2008. Climate scenarios of sea level rise for the northeast Atlantic ocean: a study including the effects of ocean dynamics and gravity changes induced by ice melt. Clim. Change 91, 351–374. http://dx.doi.org/10.1007/s10584-008-9442-9.

Katsman, C., Sterl, A., Beersma, J., van den Brink, H., Church, J., Hazeleger, W., Kopp, R., Kroon, D., Kwadijk, J., Lammersen, R., Lowe, J., Oppenheimer, M., Plag, H., Ridley, J., von Storch, H., Vaughan, D., Vellinga, P., Vermeersen, L., van de Wal, R., Weisse, R., 2011. Exploring high-end scenarios for local sea level rise to develop flood protection strategies for a low-lying delta – The Netherlands as an example. Clim. Change 109 (3–4), 617–645.

Kopp, R., Mitrovica, J., Griffies, S., Yin, J., Hay, C., Stouffer, R., 2010. The impact of Greenland melt on local sea levels: a partially coupled analysis of dynamic and static equilibrium effects in idealized water-hosing experiments. Clim. Change 103 (3), 619–625.

Lorbacher, K., Marsland, S.J., Church, J.A., Griffies, S.M., Stammer, D., Rapid barotropic sea level rise from ice sheet melting. J. Geophys. Res.: Oceans 117 (C6). http://dx.doi.org/10.1029/2011JC007733.

Madec, G., 2008. NEMO ocean engine, Note du Pole de modelisation, Institut Pierre-Simon Laplace (IPSL), France, 27, pp. 1288–1619.

Morales Maqueda, M., Fichefet, T., 1997. Sensitivity of a global sea ice model to the treatment of ice thermodynamics and dynamics. J. Geophys. Res. 102 (646), 609–612.

Morales Maqueda, M., Legat, V., Bouillon, S., Fichefet, T., 2009. An elastic–viscous–plastic sea ice model formulated on Arakawa b and c grid. vol. 27, 174–184. doi:http://dx.doi.org/10.1016/j.ocemod.2009.01.004.

Marsh, R., Desbruyères, D., Bamber, J.L., de Cuevas, B.A., Coward, A.C., Aksenov, Y., 2010. Short-term impacts of enhanced Greenland freshwater fluxes in an eddy-permitting ocean model. Ocean Sci. 6 (3), 749–760. http://dx.doi.org/10.5194/os-6-749-2010.

Martin, T., Adcroft, A., 2010. Parameterizing the fresh-water flux from land ice to ocean with interactive icebergs in a coupled climate model. Ocean Modell. 34 (34), 111–124, <http://dx.doi.org/10.1016/j.ocemod.2010.05.001>.

Meehl, G., Stocker, T.F., Collins, W.D., Friedlingstein, P., Gaye, A.T., Gregory, J.M., Kitoh, A., Knutti, R., Murphy, J.M., Noda, A., Raper, S.C.B., Watterson, I.G., Weaver, A.J., Zhao, Z., 2007. Climate Change 2007: The Physical Science Basis. In: Contribution of Working Group 1 to the Fourth Assessment Report of the Intergovernmental Panel on Climate Change. Cambridge University Press.

Mernild, S.H., Liston, G.E., 2012. Greenland freshwater runoff. Part II: Distribution and trends, 1960–2010. J. Clim. 25, 6015–6035. http://dx.doi.org/10.1175/JCLI-D-11-00592.1.

Motyka, R.J., Truffer, M., Fahnestock, M., Mortensen, J., Rysgaard, S., Howat, I., 2011. Submarine melting of the 1985 Jakobshavn Isbr floating tongue and the triggering of the current retreat. J. Geophys. Res. 116 (F1), F01007. http://dx.doi.org/10.1029/2009jf001632.

Pfeffer, W.T., Harper, J.T., O'Neel, S., 2008. Kinematic constraints on glacier contributions to 21st-century sea-level rise. Science 321 (5894), 1340–1343. http://dx.doi.org/10.1126/science.1159099.

Pritchard, H.D., Arthern, R.J., Vaughan, D.G., Edwards, L.A., 2009. Extensive dynamic thinning on the margins of the Greenland and Antarctic ice sheets. Nature 7266, 971–975. http://dx.doi.org/10.1038/nature08471.

Rignot, E., 2006. Changes in ice dynamics and mass balance of the Antarctic, ice sheet. Philos. Trans. R. Soc. London, Ser. A 364, 1637–1656.

Rignot, E., Jacobs, S.S., 2002. Rapid bottom melting widespread near Antarctic ice sheet grounding lines. Science 296 (5575), 2020–2023. http://dx.doi.org/10.1126/science.1070942.

Rignot, E., Kanagaratnam, P., 2006. Changes in the velocity structure of the Greenland ice sheet. Science 311, 986–990.

Rignot, E., Bamber, J.L., van den Broeke, M.R., Davis, C., Li, Y., van de Berg, W.J., van Meijgaard, E., 2008. Recent Antarctic ice mass loss from radar interferometry and regional climate modelling. Nat. Geosci. 1 (2), 106–110. http://dx.doi.org/10.1038/ngeo102.

Rignot, E., Koppes, M., Velicogna, I., 2010. Rapid submarine melting of the calving faces of West Greenland glaciers. Nat. Geosci. 3 (3), 187–191. http://dx.doi.org/10.1038/ngeo765.

Rignot, E., Velicogna, I., van den Broeke, M.R., Monaghan, A., Lenaerts, J., 2011. Acceleration of the contribution of the Greenland and Antarctic ice sheets to sea level rise. Geophys. Res. Lett. 38, L05503. http://dx.doi.org/10.1029/2011GL046583.

Rignot, E., Jacobs, S., Mouginot, J., Scheuchl, B., 2013. Ice-shelf melting around Antarctica. Science 341 (6143), 266–270. http://dx.doi.org/10.1126/science.1235798.

Rye, C.D., Garabato, A.C.N., Holland, P., Meredith, M., Nurser, A.G., Coward, A.C., Webb, D.J., 2014. Evidence of increased glacial melt in Antarctic coastal sea level rise. Nat. Geosci., accepted for publication.

Scambos, T.A., Bohlander, J.A., Shuman, C.A., Skvarca, P., Glacier acceleration and thinning after ice shelf collapse in the Larsen B embayment, Antarctica. Geophys. Res. Lett. 31 (18). http://dx.doi.org/10.1029/2004GL020670.

Shepherd, A., Wingham, D., 2007. Recent sea-level contributions of the Antarctic and Greenland ice sheets. Science 315 (5818), 1529–1532. http://dx.doi.org/10.1126/science.1136776.

Shepherd, A., Ivins, E.R., A, G., Barletta, V.R., Bentley, M.J., Bettadpur, S., Briggs, K.H., Bromwich, D.H., Forsberg, R., Galin, N., Horwath, M., Jacobs, S., Joughin, I., King, M.A., Lenaerts, J.T.M., Li, J., Ligtenberg, S.R.M., Luckman, A., Luthcke, S.B., McMillan, M., Meister, R., Milne, G., Mouginot, J., Muir, A., Nicolas, J.P., Paden, J., Payne, A.J., Pritchard, H., Rignot, E., Rott, H., Sørensen, L.S., Scambos, T.A., Scheuchl, B., Schrama, E.J.O., Smith, B., Sundal, A.V., van Angelen, J.H., van de Berg, W.J., van den Broeke, M.R., Vaughan, D.G., Velicogna, I., Wahr, J., Whitehouse, P.L., Wingham, D.J., Yi, D., Young, D., Zwally, H.J., 2012. A reconciled estimate of ice-sheet mass balance. Science 338 (6111), 1183–1189. http://dx.doi.org/10.1126/science.1228102.

Spence, P., Saenko, O.A., Sijp, W., England, M.H., 2013. North Atlantic climate response to lake Agassiz drainage at coarse and ocean eddy-permitting resolutions. J. Clim. 26 (8), 2651–2667. http://dx.doi.org/10.1175/JCLI-D-11-00683.1.

Stammer, D., Agarwal, N., Herrmann, P., Köhl, A., Mechoso, C., 2011. Response of a coupled ocean–atmosphere model to Greenland ice melting. Surv. Geophys., 1–22.

Swingedouw, D., Rodehacke, C.B., Behrens, E., Menary, M., Olsen, S.M., Gao, Y., Mikolajewicz, U., Mignot, J., Biastoch, A., 2013. Decadal fingerprints of freshwater discharge around Greenland in a multi-model ensemble. Clim. Dyn. 41, 695–720. http://dx.doi.org/10.1007/s00382-012-1479-9.

Taylor, K.E., Stouffer, R.J., Meehl, G.A., 2012. An overview of cmip5 and the experiment design. Bull. Am. Meteorol. Soc. 93 (4), 485–498. http://dx.doi.org/10.1175/BAMS-D-11-00094.1.

Thomas, R., Frederick, E., Krabill, W., Manizade, S., Martin, C., 2006. Progressive increase in ice loss from Greenland. Geophys. Res. Lett. 33 (10), L10503+. http://dx.doi.org/10.1029/2006GL026075.

Thomas, R., Frederick, E., Krabill, W., Manizade, S., Martin, C., 2009. Recent changes on Greenland outlet glaciers. J. Glaciol. 55 (189), 147–162.

Valcke, S., Caubel, A., Vogelsang, R., Declat, D., 2004. OASIS 3 user's guide, Technical Report TR/CMGC/04/68, CERFACS Toulouse, France.

Van Den Broeke, M.R., Bamber, J., Lenaerts, J., Rignot, E., 2011. Ice sheets and sea level: thinking outside the box. Surv. Geophys. 32 (4–5), 495–505.

van den Hurk, B., Tank, A.K., Lenderink, G., van Ulden, A., van Oldenborgh, G., Katsman, C., van den Brink, H., Keller, F., Bessembinder, J., Burgers, G., Komen, G., Hazeleger, W., Drijfhout, S., 2007. New Climate Change Scenarios for The Netherlands. vol. 56, no. 4, pp. 27–33.

Wang, C., Beckmann, A., 2007. Investigation of the impact of Antarctic ice-shelf melting in a global ice–ocean model (ORCA2-LIM). Ann. Glaciol. 1, 78–82 (2007-10-01T00:00:00).

Weijer, W., Maltrud, M.E., Hecht, M.W., Dijkstra, H.A., Kliphuis, M.A., Response of the Atlantic ocean circulation to Greenland ice sheet melting in a strongly-eddying ocean model, Geophys. Res. Lett. 39 (9). http://dx.doi.org/10.1029/2012GL051611.